POLITECNICO DI TORINO
Repository ISTITUZIONALE

Size effects on spheroidal voids by Finite Fracture Mechanics and application to corrosion pits

Original
Size effects on spheroidal voids by Finite Fracture Mechanics and application to corrosion pits / Ferrian, F., Chao Correas, A., Cornetti, P., Sapora, A.. - In: FATIGUE & FRACTURE OF ENGINEERING MATERIALS & STRUCTURES. - ISSN 8756-758X. - 46:3(2023), pp. 875-885. [10.1111/ffe.13902]

Availability:
This version is available at: 11583/2975829 since: 2023-02-09T08:32:01Z

Publisher:
WILEY

Published
DOI:10.1111/ffe.13902

Terms of use:

This article is made available under terms and conditions as specified in the corresponding bibliographic description in the repository

Publisher copyright

(Article begins on next page)

27 November 2026

Check for updates

Received: 28 September 2022 | Revised: 7 November 2022 | Accepted: 11 November 2022

DOI: 10.1111/ffe.13902

ORIGINAL ARTICLE

FFEMS Fatigue & Fracture of Engineering Materials & Structures WILEY

Size effects on spheroidal voids by Finite Fracture Mechanics and application to corrosion pits

Francesco Ferrian[1] | **Arturo Chao Correas**[1,2] | **Pietro Cornetti**[1] | **Alberto Sapora**[1]

[1]Department of Structural, Geotechnical and Building Engineering, Politecnico di Torino, Turin, Italy

[2]Elasticity and Strength of Materials Group, School of Engineering, Universidad de Sevilla, Seville, Spain

Correspondence
Francesco Ferrian, Department of Structural, Geotechnical and Building Engineering, Politecnico di Torino, Corso Duca degli Abruzzi 24, 10129, Turin, Italy.
Email: francesco.ferrian@polito.it

Funding information
Marie Skłodowska Curie, Grant/Award Number: 861061

Abstract

The present work aims at investigating the failure size effect of a spheroidal void in an infinite linear elastic solid under remote tension by means of the coupled Finite Fracture Mechanics (FFM) approach. The opening stress field and the stress intensity factor (SIF) of an annular crack surrounding the cavity —necessary for the FFM implementation— are obtained numerically through parametric axisymmetric finite element analyses (FEAs): The spheroid aspect ratio is varied between 0.1 and 10 and Poisson's ratio between 0.1 and 0.5. Accordingly, semi-analytical functions approximating the stress concentration factor and the SIF are put forward. Finally, the failure size effect on spheroidal voids is reported, and FFM predictions are compared with experimental results on the fatigue limit arising from corrosion pits, showing a fairly good agreement.

KEYWORDS

axisymmetric FEA, brittle failure, corrosion pit, fatigue limit, FFM, size effect, spheroidal void

1 | INTRODUCTION

Finite Fracture Mechanics (FFM)[1,2] is a coupled fracture initiation criterion that allows to provide strength predictions based on the simultaneous fulfilment of a stress condition and the energy balance, thus presenting an intrinsic physical meaning. In contrast to Linear Elastic Fracture Mechanics (LEFM), which assumes crack growth to develop continuously, FFM rests on the assumption of finite crack advance. This feature is shared with other nonlocal models previously proposed, which can be grouped in the framework of the Theory of Critical Distances (TCD),[3,4] in turn inspired by the works of Hashin[5] and Kim and Nairn.[6] Unlike these approaches, according to which the crack advance is a material property, FFM involves a structural crack extension, since dependent on geometric characteristics and loading conditions as well.

All in all, these features enable FFM to provide reliable failure estimations for plain, cracked, and notched elements: In comparison, LEFM only works for geometries with a sufficiently large crack.[7,8] Indeed, FFM is able to catch the transition from strength to toughness-governed failure regimes as the characteristic size of the stress-raiser varies. With the focus on the size effect of failure, FFM has been recently applied to brittle materials in presence of circular holes,[9–12] square notches,[13–15] Penny-shaped cracks,[16] and spherical cavities.[17] Likewise, FFM has been proved to provide predictions close to the well-established cohesive zone model.[12,18–20]

This is an open access article under the terms of the Creative Commons Attribution-NonCommercial-NoDerivs License, which permits use and distribution in any medium, provided the original work is properly cited, the use is non-commercial and no modifications or adaptations are made.
© 2023 The Authors. Fatigue & Fracture of Engineering Materials & Structures published by John Wiley & Sons Ltd.

14602695, 2023, 3, Downloaded from https://onlinelibrary.wiley.com/doi/10.1111/ffe.13902 by Politecnico Di Torino Sist. Bibl Del Polit Di Torino, Wiley Online Library on [09/02/2023]. See the Terms and Conditions (https://onlinelibrary.wiley.com/terms-and-conditions) on Wiley Online Library for rules of use; OA articles are governed by the applicable Creative Commons License

Although initially proposed and applied only to static problems, FFM was later extended to assess the fatigue limit of structural components. Whereas the static formulation requires the knowledge of the material ultimate tensile strength and of the fracture toughness, both the plain fatigue limit and the threshold value of the stress intensity factor range are needed in the fatigue regime. In this field, FFM has been applied to different notched geometries under either mode I[21–23] or mode III[24] loading conditions.

In the framework of fatigue failure, one of the most important issues is that related to corrosion pitting. This phenomenon is of great concern, for instance, for high-strength steel wires[25] and aluminum aerospace components,[26] or to structures under intense and unsteady high-frequency fluid–structure interactions, like turbine blades.[27,28] Corrosion is a chemical process that causes the gradual weakening of solid matter, with great impact to metallic components. Its appearance and evolution is influenced by many different parameters, including material composition, environment, temperature, and surface conditions. In particular, corrosion pitting is a very localized and critical form of damage. Pits are small and difficult to detect, and as stress raisers, they can lead to the sudden brittle failure of structures and mechanical components while stressed well under their design load.

Studies focused on the topic have been proposed since the middle of the last century, by approximating the pit shape as in between hemispherical and hemispheroidal. Eubanks[29] and Fujita et al.,[30] for instance, derived the analytical stress distribution given by a hemispherical hole under all-around remote tension. More recent works focused on the estimation of the stress concentration factor K_t, that is the ratio between the maximum value of the stress at the pit surface and the nominal stress on the gross section area, through three-dimensional (3D) finite element analyses (FEAs). To cite but a few, Huang et al.[31] assessed K_t for pits under uniaxial tension as a function of the geometry. Similarly, Cerit et al.[32] and Jie and Susmel[25] estimated K_t for semi-elliptical cavities and proposed some analytical approximate expressions. On the down side, precise 3D FEAs are computationally expensive and do not result adequate for preliminary sizing of structural components, especially considering that K_t based studies are not able to catch any size-effect according to classical linear elasticity.[33]

To simplify the analysis, Härkegård et al.[34] approximated the fatigue behavior of a hemispherical pit by that of a spherical cavity in an infinite tensile body, whose stress solution is known analytically. Under this assumption, the fatigue limit was estimated using different methods, including Smith-Miller's model,[35] which considers the pit equivalent to a crack defined by its axial projection, and Murakami's area model,[36] which takes into account the area of the defect projected along the direction of the maximum normal stress. Härkegård[37] extended the analysis using also FKM "support factor," according to FKM Guideline[38] and applying the TCD[3] in the form of the Point Method. Accordingly, fracture takes place when the normal stress equals the tensile strength at a critical distance from the stress raiser. TCD was implemented also by Jie and Susmel[25] to provide fatigue life estimations for corrosion pits, modelled as semi-ellipsoidal cavities, but disregarding the initiation crack shape.

While therefore, on the one hand, there emerges the need to improve the model proposed by Härkegård et al.[34] by taking into account the spheroidal (and not only spherical) geometry of the pit, on the other hand, this must be done considering the appropriate shape of the onset crack.

The goal of the present study is to analyze the failure behavior of a spheroidal void in an infinite tensile domain by means of FFM. Thereby, the present study generalizes those by Cornetti and Sapora[16] on Penny-shaped cracks and by Chao Correas et al.[17] on spherical cavities, which can be seen as particular cases of spheroids: In the former, the vertical axis is null; in the latter, the two axis lengths are equal with each other. The FFM criterion is here implemented by exploiting the axisymmetric problem and, consequently, by considering an annular crack shape. Following what done by Härkegård et al.,[34] the strength estimations are compared with experimental fatigue data related to corrosion pitting on two different materials: 12% Cr martensitic[27] and 17-4PH[28] turbine-grade steels.

2 | THE ANNULAR CRACK AROUND A SPHEROIDAL CAVITY

Given a spheroidal void embodied in an infinite domain under a uniform remote stress σ_∞, applied perpendicular to the void equator plane (Figure 1), let us introduce a cylindrical coordinates system (r, θ, z) centered in the spheroid. The r-θ plane thus coincides with the spheroidal equator and the z-axis with its revolution axis, in turn aligned with the remote loading. The two semi-axes normal and parallel to the loading σ_∞ are denoted by a and b, respectively.

Considering an isotropic homogenous material and given that the configuration under study is axisymmetric, an annular crack of width c is expected to initiate under Mode I opening conditions in the $z = 0$ plane, that is within the void's equator.

In the reference plane for fracture, $z = 0$, the tridimensional coordinate system (r, θ, z) can be reduced to unidimensional, the only relevant coordinate being the

14602695, 2023, 3, Downloaded from https://onlinelibrary.wiley.com/doi/10.1111/ffe.13902 by Politecnico Di Torino Sist. Bibl Del Polit Di Torino, Wiley Online Library on [09/02/2023]. See the Terms and Conditions (https://onlinelibrary.wiley.com/terms-and-conditions) on Wiley Online Library for rules of use; OA articles are governed by the applicable Creative Commons License

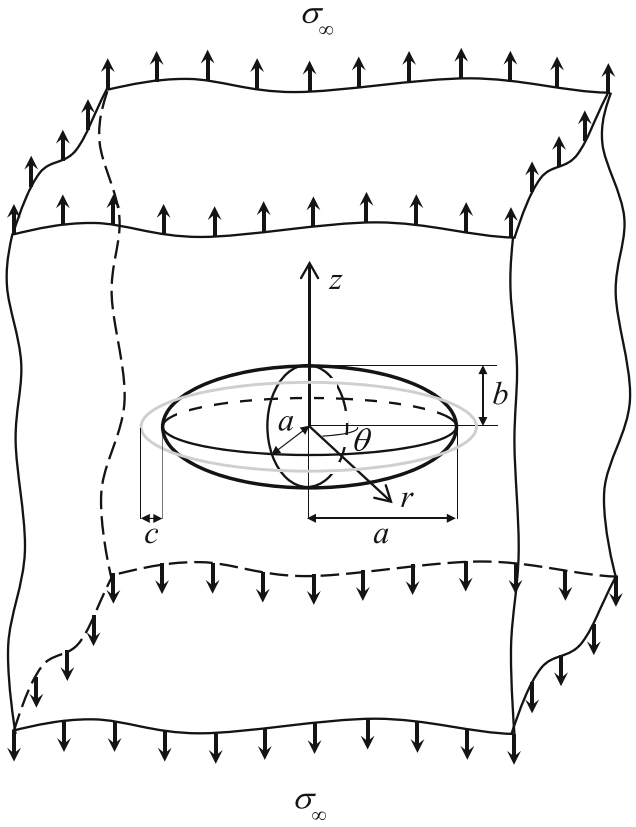


FIGURE 1 Schematic representation of a spheroidal void in an infinite tensile continuum. The annular crack of length c (grey line) surrounding the spheroidal void represents the supposed crack initiation

radial one, r. Accordingly, the stress field function of interest can be expressed as ($r \geq a$):

$$\sigma_{zz}(r) = \sigma_\infty S(r, a, b, \nu) \tag{1}$$

and the stress concentration factor K_t writes:

$$K_t = \frac{\sigma_{zz}(a)}{\sigma_\infty} \tag{2}$$

Note that the shape function S (r, a, b, ν) in Equation (1) depends on the geometrical dimensions of the void, as well as on the material through Poisson's ratio ν. In this work, S is estimated through a parametrized and axisymmetric FEA using ANSYS® code. In order to mimic the infinite geometry assumption, the height h and the width w of the domain are considered at least 10 times greater than the maximum spheroidal axis a or b. Vertical symmetry in the setup is exploited, and just the upper half is modelled. Axisymmetric quadratic elements are used, with eight nodes and characterized by a reduced integration solution scheme. The FE mesh pattern used to calculate the stress field is analogous to that used to calculate the SIF (see Section 2.1), but for the presence of the crack and the respective localized mesh refinement at the crack tip. The minimum dimension of the finite elements at the stress concentration region is determined through a convergent analysis and set equal to 0.01 a.

Varying Poisson's ratio ν from 0.1 to 0.5, the stress field is evaluated for different ratios b/a ranging from 0.1 to 10. Results are presented in Figure 2A. As ν increases, the stress field intensifies for any aspect ratio. However, the dependence of the stress field on ν is limited in magnitude. Indeed, considering $b/a = 0.5$, the peak stress value obtained for $\nu = 0.5$ is nearly 9% higher than the corresponding one for $\nu = 0.1$. This difference progressively decreases as r increases, the stress field quickly converging to the applied loading σ_∞.

Figure 2B shows the behavior of K_t as a function of ν and b/a. This trend can be approximated by the following expression, which we propose on the basis of a nonlinear fitting on numerical results (typical errors lower than 5%):

$$K_t = 1 + \frac{m}{(b/a)^n} \tag{3a}$$

$$m = 0.23\nu^2 + 0.27\nu + 1.0 \tag{3b}$$

$$n = -0.03\nu^2 - 0.11\nu + 1.1 \tag{3c}$$

Note that, for the spherical case ($b/a = 1$), Equation (3) provides close results to those by the (exact) analytical expression (4),[39] with a maximum deviation of 3% for $\nu = 0.2$:

$$K_t = \frac{3(9 - 5\nu)}{2(7 - 5\nu)} \tag{4}$$

2.1 | Stress intensity factor

The SIF K_I^{sph} for an annular crack of width c surrounding the spheroidal void (Figure 1), on the basis of the works by Fett[40] and Chao Correas et al.,[17] can be achieved considering the interpolation between two limit cases: (i) the edge crack and (ii) the Penny shaped crack. Indeed, when a, $b >> c$, the configuration resembles an edge crack of length c (Figure 3A), while if a, $b << c$, it tends to a Penny shaped one with radius $a + c$ (Figure 3B).

Based on the above considerations, we can express the SIF K_I^{sph} as follows:

$$\begin{cases} K_I^{sph} = \sigma_\infty \sqrt{\pi c} F_I^{sph} \\ F_I^{sph} = F_I^{EC} \gamma(c, a, b, \nu) + F_I^{PC}[1 - \gamma(c, a, b, \nu)] \end{cases} \tag{5}$$

14602695, 2023, 3, Downloaded from https://onlinelibrary.wiley.com/doi/10.1111/ffe.13902 by Politecnico Di Torino Sist. Bibl Del Polit Di Torino, Wiley Online Library on [09/02/2023]. See the Terms and Conditions (https://onlinelibrary.wiley.com/terms-and-conditions) on Wiley Online Library for rules of use; OA articles are governed by the applicable Creative Commons License

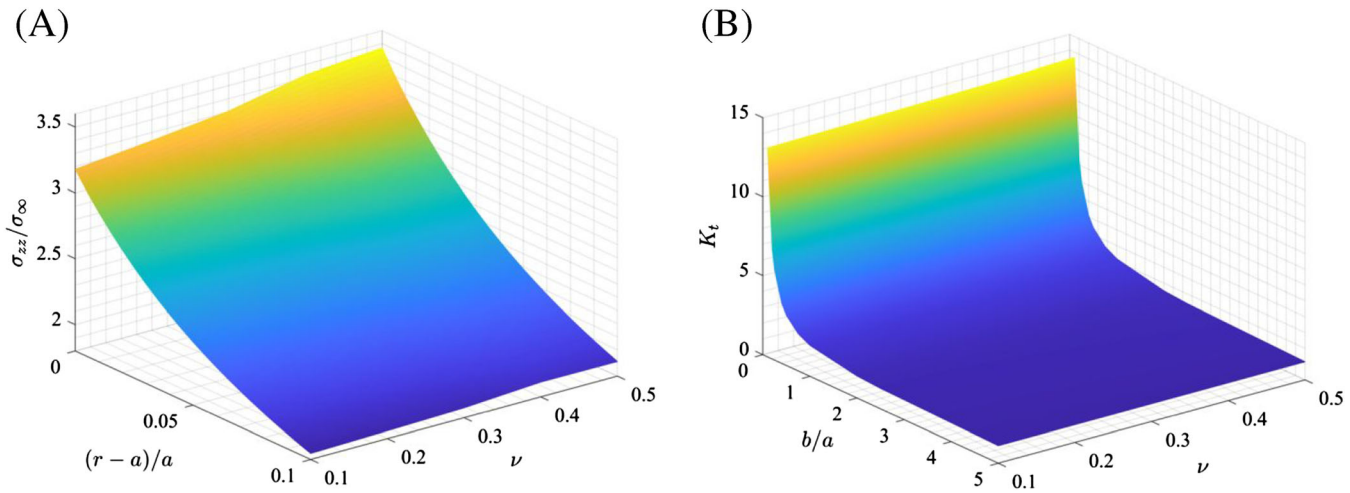


FIGURE 2 (A) Dimensionless longitudinal stress field for $b/a = 0.5$ as ν varies from 0.1 to 0.5; (B) stress concentration factor K_t as a function of b/a and ν [Colour figure can be viewed at wileyonlinelibrary.com]

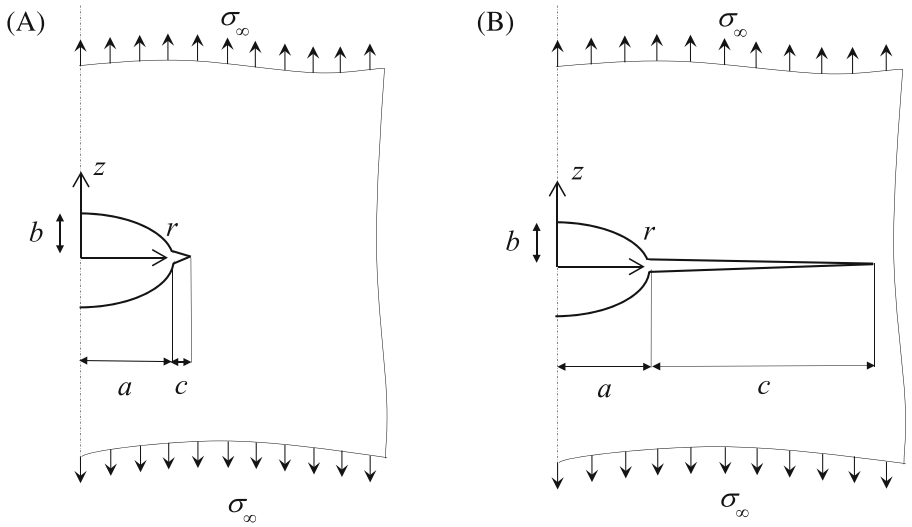


FIGURE 3 Limit cases for the SIF: (A) edge crack for $a, b >> c$; (B) Penny shaped crack for $a, b << c$

where F_I^{sph}, F_I^{EC}, and F_I^{PC} are the shape functions in the spheroidal, edge cracked, and Penny-shaped cracked configurations, respectively, whereas $\gamma\ (c, a, b, \nu)$ is the interpolation function.

In accordance to previous observations, $\gamma = 1$ when $a << b$: Thus, $F_I^{sph} = F_I^{EC}$, with F_I^{EC} given by the well-known factor 1.122 times the stress concentration factor K_t. On the other hand, $a >> b$ requires $\gamma = 0$ to achieve $F_I^{sph} = F_I^{PC}$. The shape function F_I^{PC} can be obtained through the method mentioned in Fett[40]:

$$F_I^{PC} = \int_a^{a+c} \sigma_{zz}(r) h_{PC}(r, a, c) dr \tag{6}$$

where the weight function $h_{PC}(r, a, c)$ is defined as

$$h_{PC}(r, a, c) = \frac{2r}{\sqrt{\pi(c+a)\left[(c+a)^2 - r^2\right]}} \tag{7}$$

As concerns the function γ for intermediate geometries, Chao Correas et al.[17] proposed an interpolating expression based on axisymmetric FEA results for the spherical case ($a = b = R$):

$$\gamma(c, R) = \left(\frac{R}{R+5c}\right)^2 \tag{8}$$

Equation (8) fulfils the limit cases of an edge crack and a Penny shaped crack, since $\gamma \to 1$ for $c/R \to 0$, and $\gamma \to 0$ for $c/R \to \infty$. Note that Equation (8) is independent from

14602695, 2023, 3, Downloaded from https://onlinelibrary.wiley.com/doi/10.1111/ffe.13902 by Politecnico Di Torino Sist. Bibl Del Polit Di Torino, Wiley Online Library on [09/02/2023]. See the Terms and Conditions (https://onlinelibrary.wiley.com/terms-and-conditions) on Wiley Online Library for rules of use; OA articles are governed by the applicable Creative Commons License

v, reflecting the weak dependence on Poisson's ratio detected numerically.

We can herein generalize Equation (8) for the spheroidal configuration as:

$$\gamma(c, a, b, v) = \left[\frac{a}{a + f_\sigma(a,\ b,\ v)c}\right]^2 \tag{9}$$

with:

$$f_\sigma(a, b, v) = \left(\frac{Q \cdot a}{b}\right)^P \tag{10}$$

Equation (10) satisfies the conditions $f_\sigma(a << b) = 0$ and $f_\sigma(a >> b) = \infty$.

To evaluate the parameters P and Q, parametrized axisymmetric FEAs using ANSYS® code are performed to determine different K_I^{sph} values. The mesh and the model schematic definition are represented in Figure 4. Once again, the height h and the width w of the model are considered at least 10 times greater than the maximum spheroidal semi-axes to ensure negligible edge-effects. Axisymmetric quadratic elements are used, with 8 nodes and characterized by a reduced integration solution scheme. To reduce the computational cost yet keeping the accuracy, following a convergence analysis, the mesh is refined within a semi-circle of radius $0.5c$ centered at the crack tip: Therein, the minimum dimension of the elements is set to $0.01c$.

Now, it is seen that the SIF problem, that is, the estimation of P and Q, is doubly parametrized, since it depends on both b/a and c/a ratios. In this sense, for each b/a from 0.1 to 10, the SIF magnitude is obtained for different c/a, also within the range from 0.1 to 10. Subsequently, the parameters P and Q are determined on the basis of best fitting to the numerical results. This procedure is repeated for five different Poisson's ratios ($v = 0.1$, 0.2, 0.3, 0.4, 0.5), showing that P and Q do not show a strong dependence on v. For this reason, the average values of those estimated for the different values of v, namely, $P = 1.86$ and $Q = 2.70$, are considered. This choice leads, for the spherical case, to $f_\sigma \approx 6.3$ (Equation 10) which slightly differs from the factor 5 proposed[17] in Equation (8).

3 | FINITE FRACTURE MECHANICS (FFM)

According to Finite Fracture Mechanics (FFM), crack propagation occurs when a stress and an energy conditions are simultaneously fulfilled. FFM was proposed and consolidated in the static regime[1,2] and recently extended to the fatigue framework.[22,23] Following Leguillon's approach,[1] the stress requirement imposes that the normal stress range $\Delta\sigma_{zz}$ must exceed the plain fatigue limit $\Delta\sigma_0$ over a finite distance l. Under linear elastic assumptions, the discrete energy balance can be defined through the J-integral range formalism, which involves the SIF range ΔK_I and its threshold value ΔK_{th}. Particularizing the FFM formulation to the present geometry, which turns out to be positive, the two conditions can be cast in the following form:

$$\begin{cases} \Delta\sigma_{zz}(a + l_c) = \Delta\sigma_0 \\ \displaystyle\int_0^{l_c} \left[\Delta K_I^{sph}(c)\right]^2 2\pi(c + a)dc = \pi\left[(a + l_c)^2 - a^2\right]\Delta K_{th}^2 \end{cases} \tag{11}$$

The energy balance can also be coupled with an average stress condition, requiring that the average longitudinal

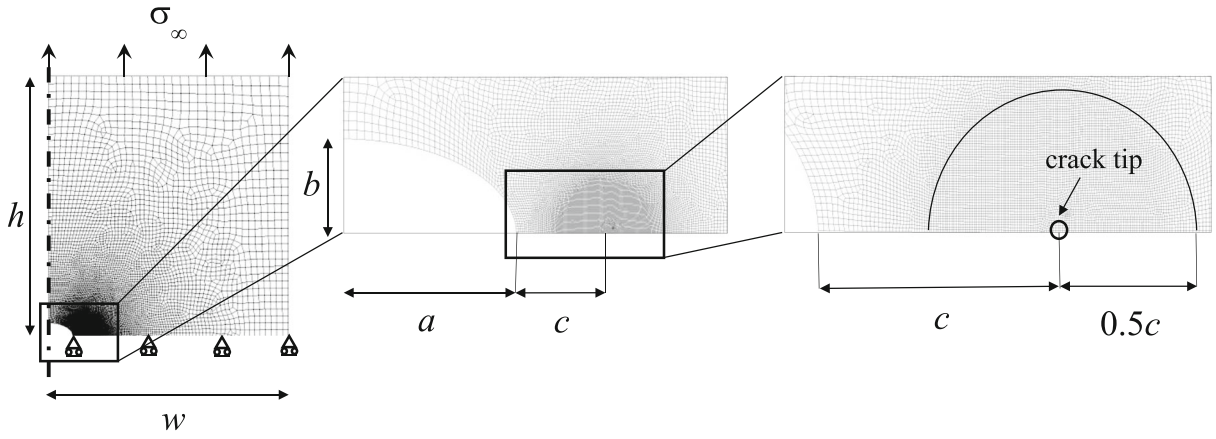


FIGURE 4 Finite element model implemented to determine the SIF K_I^{sph} for $b/a = 0.5$

14602695, 2023, 3, Downloaded from https://onlinelibrary.wiley.com/doi/10.1111/ffe.13902 by Politecnico Di Torino Sist. Bibl Del Polit Di Torino, Wiley Online Library on [09/02/2023]. See the Terms and Conditions (https://onlinelibrary.wiley.com/terms-and-conditions) on Wiley Online Library for rules of use; OA articles are governed by the applicable Creative Commons License

stress range over a distance l must exceed the plain fatigue limit $\Delta\sigma_0$. Accordingly, the avg-FFM approach writes:

$$\begin{cases} \int_a^{a+l_c} \Delta\sigma_{zz}(r)2\pi r dr = \pi\left[(a+l_c)^2 - a^2\right]\Delta\sigma_0 \\ \int_0^{l_c} \left[\Delta K_I^{sph}(c)\right]^2 2\pi(c+a)dc = \pi\left[(a+l_c)^2 - a^2\right]\Delta K_{th}^2 \end{cases} \tag{12}$$

Both FFM formulations (11) and (12) are thus represented by a system of two equations in two unknowns: the fatigue limit $\Delta\sigma_f$ and the critical crack advancement l_c, which reveals to be a structural parameter, since dependent on both material and geometry.

3.1 | FFM implementation

Introducing Equations (1) and (5) into Equation (11), the critical conditions ($\Delta\sigma_\infty = \Delta\sigma_f$) predicted by FFM follow:

$$\begin{cases} \dfrac{\Delta\sigma_f}{\Delta\sigma_0} = \dfrac{1}{S(a+l_c,\ a,\ b,\ \nu)} \\ \dfrac{\Delta\sigma_f}{\Delta\sigma_0} = \sqrt{\dfrac{l_{th}\left(l_c^2+2al_c\right)}{2\pi\displaystyle\int_0^{l_c} c(c+a)\left[F_I^{sph}(c,\ a,\ b,\ \nu)\right]^2 dc}} \end{cases} \tag{13}$$

where $l_{th} = (\Delta K_{th}/\Delta\sigma_0)^2$ generalizes the well-known Irwin's length defined in the static framework.[22] FFM estimations are obtained by equaling the right-hand sides of system (13): The solution of an implicit nonlinear equation yields the critical crack advancement l_c. This value is then introduced into one of the two equations in (13) to get the corresponding dimensionless fatigue limit. On the other hand, considering the avg-FFM approach (Equation 12), the critical conditions are found through the following system:

$$\begin{cases} \dfrac{\Delta\sigma_f}{\Delta\sigma_0} = \dfrac{l_c^2+2al_c}{2\displaystyle\int_a^{a+l_c} S(r,\ a,\ b,\ \nu)rdr} \\ \dfrac{\Delta\sigma_f}{\Delta\sigma_0} = \sqrt{\dfrac{l_{th}\left(l_c^2+2al_c\right)}{2\pi\displaystyle\int_0^{l_c} c(c+a)\left[F_I^{sph}(c,\ a,\ b,\ \nu)\right]^2 dc}} \end{cases} \tag{14}$$

which can be solved analogously to Equation (13). Strength predictions for different b/a ratios varying from 0 (Penny-shaped crack) to 10 (very prolate spheroid) are plotted in Figure 5 considering a constant Poisson's ratio $\nu = 0.3$. As evident, the normalized failure stress $\Delta\sigma_f/\Delta\sigma_0$ increases for higher b/a ratios, that is for more prolate spheroids. Clearly, the solution herein obtained for $b/a = 0$ coincides with the Penny shaped crack solution reported by Cornetti and Sapora.[16]

The influence of Poisson's ratio on the strength scaling is highlighted in Figure 6A, where the theoretical

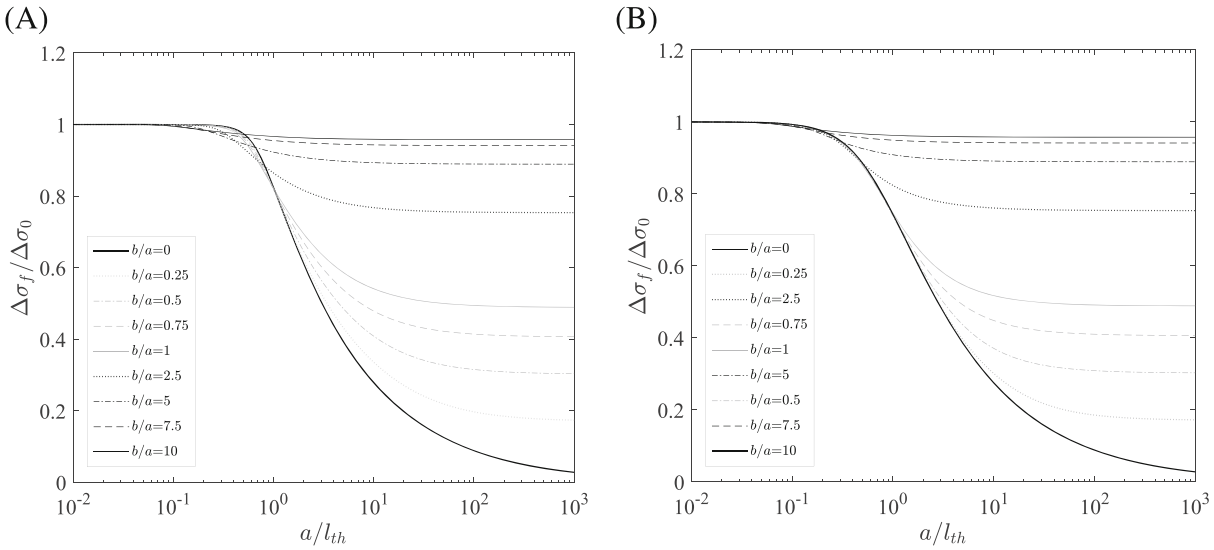


FIGURE 5 Fatigue strength estimations provided by (A) FFM and (B) avg-FFM for different ratios b/a over the range 0 to 10. Poisson's ratio is fixed, $\nu = 0.3$

14602695, 2023, 3, Downloaded from https://onlinelibrary.wiley.com/doi/10.1111/ffe.13902 by Politecnico Di Torino Sist. Bibl Del Polit Di Torino, Wiley Online Library on [09/02/2023]. See the Terms and Conditions (https://onlinelibrary.wiley.com/terms-and-conditions) on Wiley Online Library for rules of use; OA articles are governed by the applicable Creative Commons License

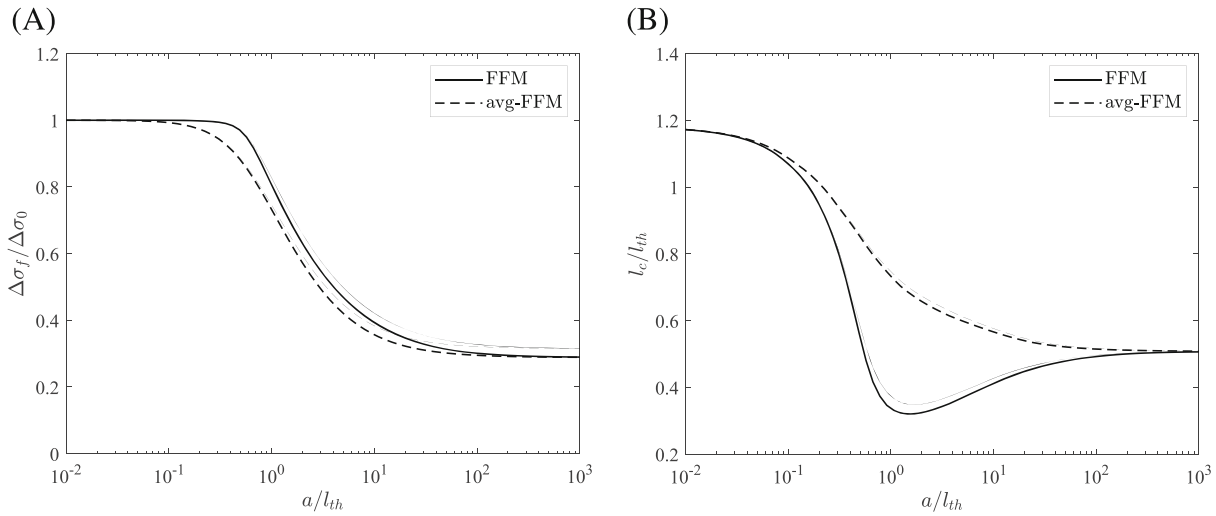


FIGURE 6 (A) Fatigue strength estimations $\Delta\sigma_f/\Delta\sigma_0$ and (B) normalized critical crack advancement l_c/l_{th} by FFM and avg-FFM, for $b/a = 0.5$: $\nu = 0.1$ (thin line) and $\nu = 0.5$ (thick line)

estimations are plotted for $\nu = 0.1$ and $\nu = 0.5$, fixing $b/a = 0.5$. As expected, avg-FFM provides the most conservative estimations. Besides, lower effective strength predictions are obtained increasing Poisson's ratio. Nevertheless, the dependency of the results on ν is again small, and it increases as a/l_{th} increases, until becoming nearly constant from $a/l_{th} \approx 10^2$, that is, when the solution becomes governed by the stress concentration factor K_t.

In Figure 6B, the normalized critical crack advancement l_c/l_{th} is reported as function of a/l_{th}. Avg-FFM provides higher l_c/l_{th} values with respect to FFM, but both approaches converge to $3\pi/8$ for $a/l_{th} \to 0$ and to $2/1.122^2\pi$ for $a/l_{th} \to \infty$. These extreme values coincide with those obtained for a Penny shaped crack[16] and an edge crack,[2] respectively. Furthermore, once again, the influence of Poisson's ratio on l_c/l_{th} is small and limited —in this case— to the transition zone between the voidless and large-size solutions, similarly to the case of spherical voids.

4 | COMPARISON WITH EXPERIMENTAL DATA

Several works in the scientific literature addressed the evaluation of stress concentration due to the presence of corrosion pits.[25,32] As outlined in Section 1, corrosion pitting is a localized and accelerated dissolution process —mainly affecting metals— that occurs as a result of a damage of the protective passive film on the material surface. This phenomenon is one of the most common failure mechanisms in presence of a corrosive environment. In a recent work, Härkegård et al.[34] approximated the fatigue behavior of a surface pit by that of a spherical void in an infinite body. This approximation allows to overcome the drawback related to the high computational cost of a 3D FEA because the geometry becomes axisymmetric. Note that differences between edge and centre notched geometries are usually small: For $b/a = 1$, the deviation of the stress concentration factor K_t is 7% for $\nu = 0.25$,[29] whereas for $b/a \to 0$, the deviation of the SIF is around 12%.[41] Hence, we herein make the same assumption, approximating the edge hemispheroidal geometry by a central spheroidal one.

Following this approach, the axisymmetric model presented in Figure 1 is exploited. Fatigue strength estimations obtained for a spheroidal void are hence compared with experimental fatigue data on steel specimens in presence of corrosion pits.[27,28]

Experimental tests on specimens of a 12% Cr martensitic steel for steam turbine blades ($E = 200$ GPa and $\nu = 0.3$), with a single corrosion pit, were carried out by Salzman et al.[27] Fatigue results were generated by means of ultrasonic fatigue testing carried out in air at 90°C. Three different stress ratios were considered: $R_L = 0.05$, 0.5, and 0.8. For each R_L, the mechanical properties of the materials are reported in Table 1: They were evaluated experimentally in the reference article.[27]

The fatigue limit $\Delta\sigma_0$ refers to 10^9 cycles and is based on S-N curves covering the range 10^4–10^9 cycles. Test results are divided into three different categories: (i) No Crack, (ii) Self Arrested Crack (SAC), and (iii) Failure. In the former case, no cracks were observed after 10^9 cycles, whereas in the second case, SAC cracks were detected after the same number of cycles. In the latter case, fatigue

14602695, 2023, 3, Downloaded from https://onlinelibrary.wiley.com/doi/10.1111/ffe.13902 by Politecnico Di Torino Sist. Bibl Del Polit Di Torino, Wiley Online Library on [09/02/2023]. See the Terms and Conditions (https://onlinelibrary.wiley.com/terms-and-conditions) on Wiley Online Library for rules of use; OA articles are governed by the applicable Creative Commons License

TABLE 1 Mechanical properties of the materials considered in the present study

Material	Reference	R_L	$\Delta\sigma_0$ (MPa)	ΔK_{th} (MPa$\sqrt{m}$)	l_{th} (mm)
12% Cr martensitic steel	Salzman et al.[27]	0.05	640	3.8	0.035
		0.5	370	2.7	0.053
		0.8	150	2.2	0.220
17-4PH steel	Schönbauer et al.[28]	0.05	769	3.3	0.019
		0.4	600	2.6	0.019

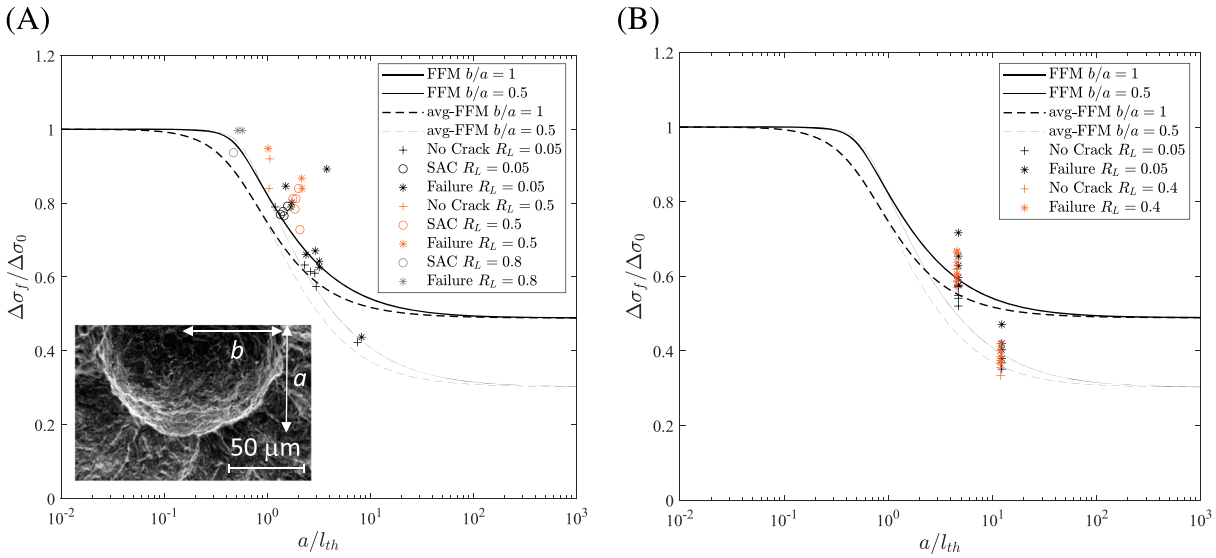


FIGURE 7 Comparison between the experimental data obtained by (A) Salzman et al.[27] and by (B) Schönbauer et al.[28] and theoretical fatigue limit estimations $\Delta\sigma_f/\Delta\sigma_0$ provided by FFM (continuous line) and avg-FFM (dashed line) for $b/a = 0.5$ (thin line) and $b/a = 1$ (thick line). The subplot in Figure 7A is re-arranged from Salzman et al.[27] [Colour figure can be viewed at wileyonlinelibrary.com]

failure occurred from 10^5 cycles upwards. The pits were characterized by a ratio $0.5 < b/a < 1$ (see the subplot of Figure 7A). Experimental data are plotted in Figure 7A, together with a schematic representation of the pit and theoretical strength estimations for $b/a = 0.5$ and 1. As expected, FFM and avg-FFM predictions reveal conservative for $b/a = 0.5$. Anyhow, the FFM approach (Equation 13) reveals to be more accurate. Despite the intrinsic uncertainty and scatter in the fatigue results, "No Crack" data generally fall in between the two FFM curves.

A second set of data obtained by Schönbauer et al.[28] is also considered. In this study, fatigue life tests were carried out in air at 90°C by means of an ultrasonic fatigue test machine on pre-pitted specimens made of 17-4PH turbine-grade steel ($E = 200$ GPa and $\nu = 0.3$). Two different stress ratios were considered, $R_L = 0.05$ and 0.4: The evaluated mechanical properties[28] are reported in Table 1. The fatigue limit $\Delta\sigma_0$ refers again to 10^9 cycles. Results were divided into "No Crack" and "Failure." In the former case, no cracks were observed after 10^9 cycles, whereas in the latter case, failure occurred for a number of cycles ranging from 10^5 to $2{\cdot}10^6$. The pits were characterized by a ratio b/a approximately variable between 0.5 and 1. Results are presented in Figure 7B: In this case, avg-FFM provides the most reliable predictions, being able to catch the transition from "No Crack" to "Failure" data. Finally, the value of the critical crack lengths l_c can be estimated from Figure 6B and Table 1 (l_{ch}) for both steels: Its value approximately ranges from 0.007 to 0.13 mm for FFM, and from 0.010 to 0.19 mm for avg-FFM.

5 | CONCLUSIONS

In this work, the size effect of a spheroidal cavity in an infinite linear elastic solid under remote tension was investigated by means of Finite Fracture Mechanics (FFM) approaches. In order to obtain the stress field and SIF expressions, necessary to apply FFM, an axisymmetric and parametric FEA was conducted using ANSYS® code, varying ν between 0.1 and 0.5, and the axis ratio $b/$

14602695, 2023, 3, Downloaded from https://onlinelibrary.wiley.com/doi/10.1111/ffe.13902 by Politecnico Di Torino Sist. Bibl Del Polit Di Torino, Wiley Online Library on [09/02/2023]. See the Terms and Conditions (https://onlinelibrary.wiley.com/terms-and-conditions) on Wiley Online Library for rules of use; OA articles are governed by the applicable Creative Commons License

a from 0.1 (an oblate spheroid) to 10 (a prolate spheroid). The SIF function related to an annular crack from the void's equator was obtained through an interpolation between two limit cases: the edge crack (very small cracks) and the Penny shaped crack (very large cracks). By approximating corrosion pits with spheroidal cavities, theoretical estimations were analyzed and compared successfully with experimental fatigue data,[27,28] resulting in improved predictive capabilities in comparison with failure/fatigue criteria already proposed in the literature. The approximation allowed us avoiding the implementation of 3D FEAs, which reveal more complex, both computationally and substantially. Indeed, the implementation of 3D FFM failure analysis for the case at hand would result in increasing complexity as for determining the finite crack growth shape, which is no more annular due to the lack of axial symmetry. A first attempt could be to assume a finite crack advance whose front is given by iso-stress lines, as proposed recently by other authors,[42] so to satisfy exactly the stress requirement. However, for larger defects, crack growth could be even different, as energy condition is expected to prevail. In this sense, further studies are in progress.

The present work constitutes a first effort towards the generalization of coupled FFM approaches to the study of spheroidal voids and of the effect of corrosion pitting on the fatigue limit. Following steps could include: (i) the implementation of Cohesive Crack Model approaches to further validate the theoretical framework; (ii) the FFM extension to determine the finite fatigue life as presented by Jie and Susmel,[25] who applied TCD to high-strength metallic cables; (iii) the investigation of the interaction between two or more pits, as presented by Chouchaoui and Pick[43] and Hou and Song.[44]

ACKNOWLEDGMENTS

This project has received funding from the European Union's Horizon 2020 research and innovation programme under the Marie Skłodowska Curie grant agreement no. 861061.



DATA AVAILABILITY STATEMENT

Data sharing is not applicable to this article as no datasets were generated or analysed during the current study.

NOMENCLATURE

a	spheroidal void semi-axis normal to the loading
b	spheroidal void semi-axis parallel to the loading
c	annular crack length
E	Young's modulus
K_t	stress concentration factor
K_I^{sph}	SIF for an annular crack of width c surrounding the spheroidal void
F_I^{sph}	SIF shape function in the spheroidal configuration
F_I^{EC}	SIF shape function in the edge cracked configuration
F_I^{PC}	SIF shape function in the Penny shaped cracked configuration
h	height of the FE geometry
l	finite crack advance
l_c	critical finite crack advance
l_{th}	Irwin's length
P,Q	coefficients of the interpolating function γ
S	stress field shape function
w	width of the FE geometry
(r, θ, z)	cylindrical coordinates system
ΔK_{th}	threshold value of the stress intensity factor range
$\Delta\sigma_f$	fatigue limit
$\Delta\sigma_0$	plain fatigue limit
γ	interpolating function for the SIF
σ_{zz}	normal stress
σ_∞	uniform remote stress
ν	Poisson's ratio

ORCID

Francesco Ferrian https://orcid.org/0000-0002-2093-5765

Alberto Sapora https://orcid.org/0000-0003-3181-3381

REFERENCES

1. Leguillon D. Strength or toughness? A criterion for crack onset at a notch. *Eur J Mech - A/Solids*. 2002;21(1):61-72.
2. Cornetti P, Pugno N, Carpinteri A, Taylor D. Finite fracture mechanics: a coupled stress and energy failure criterion. *Eng Fract Mech*. 2006;73(14):2021-2033.
3. Taylor D. *The Theory of Critical Distances*. London: Elsevier; 2007.
4. Susmel L. *Multiaxial Notch Fatigue*. Oxford: Woodhead Publishing; 2009.
5. Hashin Z. Finite thermoelastic fracture criterion with application to laminate cracking analysis. *J Mech Phys Solids*. 1996; 44(7):1129-1145.

14602695, 2023, 3, Downloaded from https://onlinelibrary.wiley.com/doi/10.1111/ffe.13902 by Politecnico Di Torino Sist. Bibl Del Polit Di Torino, Wiley Online Library on [09/02/2023]. See the Terms and Conditions (https://onlinelibrary.wiley.com/terms-and-conditions) on Wiley Online Library for rules of use; OA articles are governed by the applicable Creative Commons License

6. Kim S-R, Nairn JA. Fracture mechanics analysis of coating/substrate systems. *Eng Fract Mech*. 2000;65(5):573-593.
7. Mukhtar F, Qayyum F, Elahi H, Shah M. Studying the effect of thermal fatigue on multiple cracks propagating in an SS316L thin flange on a shaft specimen using a multi-physics numerical simulation model. *Strojniški Vestn – J Mech Eng*. 2019;(10):565-573.
8. Hussain N, Qayyum F, Pasha RA, Shah M. Development of multi-physics numerical simulation model to investigate thermo-mechanical fatigue crack propagation in an autofrettaged gun barrel. *Def Technol*. 2021;17(5):1579-1591.
9. Sapora A, Cornetti P. Crack onset and propagation stability from a circular hole under biaxial loading. *Int J Fract*. 2018;214(1):97-104.
10. Doitrand A, Leguillon D. Asymptotic analysis of pore crack initiation near a free edge. *Theor Appl Fract Mech*. 2021;116:103125.
11. Wegert ZJ, Challis VJ, Grotowski JF, Roberts AP. Explaining the competition between strength and toughness in perforated plates using computational finite fracture mechanics. *Theor Appl Fract Mech*. 2022;122:103615.
12. Ferrian F, Cornetti P, Marsavina L, Sapora A. Finite fracture mechanics and cohesive crack model: size effects through a unified formulation. *Frat Integrità Strutt*. 2022;16(61):496-509.
13. Cornetti P, Sapora A, Carpinteri A. Mode mixity and size effect in V-notched structures. *Int J Solids Struct*. 2013;50(10):1562-1582.
14. Doitrand A, Estevez R, Leguillon D. Experimental characterization and numerical modeling of crack initiation in rhombus hole PMMA specimens under compression. *Eur J Mech - a/-Solids*. 2019;76:290-299.
15. Doitrand A, Cornetti P, Sapora A, Estevez R. Experimental and theoretical characterization of mixed mode brittle failure from square holes. *Int J Fract*. 2021;228(1):33-43.
16. Cornetti P, Sapora A. Penny-shaped cracks by finite fracture mechanics. *Int J Fract*. 2019;219(1):153-159.
17. Chao Correas A, Corrado M, Sapora A, Cornetti P. Size-effect on the apparent tensile strength of brittle materials with spherical cavities. *Theor Appl Fract Mech*. 2021;116:103120.
18. García IG, Paggi M, Mantič V. Fiber-size effects on the onset of fiber–matrix debonding under transverse tension: a comparison between cohesive zone and finite fracture mechanics models. *Eng Fract Mech*. 2014;115:96-110.
19. Cornetti P, Muñoz-Reja M, Sapora A, Carpinteri A. Finite fracture mechanics and cohesive crack model: weight functions vs. cohesive laws. *Int J Solids Struct*. 2019;156–157:126-136.
20. Doitrand A, Estevez R, Leguillon D. Comparison between cohesive zone and coupled criterion modeling of crack initiation in rhombus hole specimens under quasi-static compression. *Theor Appl Fract Mech*. 2019;99:51-59.
21. Liu Y, Deng C, Gong B. Discussion on equivalence of the theory of critical distances and the coupled stress and energy criterion for fatigue limit prediction of notched specimens. *Int J Fatigue*. 2020;131:105326.
22. Sapora A, Cornetti P, Campagnolo A, Meneghetti G. Fatigue limit: crack and notch sensitivity by finite fracture mechanics. *Theor Appl Fract Mech*. 2020;105:102407.
23. Sapora A, Cornetti P, Campagnolo A, Meneghetti G. Mode I fatigue limit of notched structures: a deeper insight into finite fracture mechanics. *Int J Fract*. 2021;227(1):1-13.
24. Campagnolo A, Sapora A. A FFM analysis on mode III static and fatigue crack initiation from sharp V-notches. *Eng Fract Mech*. 2021;258:108063.
25. Jie Z, Susmel L. High-strength steel wires containing corrosion pits: stress analysis and critical distance based fatigue life estimation. *Fatigue Fract Eng Mater Struct*. 2020;43(8):1611-1629.
26. Crawford BR, Loader C, Liu QC, Harrison TJ, Sharp PK, Härkegård G. Experimental and modeling study of the effect of corrosion pitting on fatigue failure locations in aircraft components. *Adv Mat Res*. 2014;891–892:236-241.
27. Salzman R, Gandy D, Rieger N, et al. Corrosion-fatigue prediction methodology for 12% Cr steam turbine blades. In: *Volume 1: Fuels and Combustion, Material Handling, Emissions; Steam Generators; Heat Exchangers and Cooling Systems; Turbines, Generators and Auxiliaries; Plant Operations And Maintenance*. American Society of Mechanical Engineers; 2013.
28. Schönbauer BM, Stanzl-Tschegg SE, Perlega A, et al. The influence of corrosion pits on the fatigue life of 17-4PH steam turbine blade steel. *Eng Fract Mech*. 2015;147:158-175.
29. Eubanks RA. Stress concentration due to a hemispherical pit at a free surface. *J Appl Mech*. 1954;21(1):57-62.
30. Fujita T, Sadayasu T, Tsuchida E, Nakahara I. Stress concentration due to a hemispherical pit at a free surface of a thick plate under all-around tension. *Bull JSME*. 1978;21(154):561-565.
31. Huang Y, Wei C, Chen L, Li P. Quantitative correlation between geometric parameters and stress concentration of corrosion pits. *Eng Fail Anal*. 2014;44:168-178.
32. Cerit M, Genel K, Eksi S. Numerical investigation on stress concentration of corrosion pit. *Eng Fail Anal*. 2009;16(7):2467-2472.
33. Sapora A, Efremidis G, Cornetti P. Non-local criteria for the borehole problem: gradient elasticity versus finite fracture mechanics. *Mec Dent*. 2022;57(4):871-883.
34. Härkegałrd G. Short-crack modelling of the effect of corrosion pits on the fatigue limit of 12% Cr steel. *Fatigue Fract Eng Mater Struct*. 2015;38(9):1009-1016.
35. Smith RA, Miller KJ. Prediction of fatigue regimes in notched components. *Int J Mech Sci*. 1978;20(4):201-206.
36. Murakami Y. *Metal Fatigue: Effects of Small Defects and Non-Metallic Inclusions*. Elsevier; 2002.
37. Härkegård G. Modelling the effect of a spherical cavity on the fatigue limit of a 12% Cr steel. *Theor Appl Fract Mech*. 2016;84:93-97.
38. FKM-Richtlinie. In: FKM, ed. *Rechnerischer Festigkeitsnachweis Für Maschinenbauteile*. fifth ed. Frankfurt am Main; 2003.
39. Goodier JN. Concentration of stress around spherical and cylindrical inclusions and flaws. *J Appl Mech*. 1933;1(2):39-44.
40. Fett T. Stress intensity factors and weight function for a void with an annular crack. *Int J Fract*. 1994;67(2):R41-R47.
41. Tada H, Paris PC, Irwin GR. *The Stress Analysis of Cracks Handbook*. Thirded. ASME Press; 2000.
42. Doitrand A, Leguillon D. 3D application of the coupled criterion to crack initiation prediction in epoxy/aluminum

14602695, 2023, 3, Downloaded from https://onlinelibrary.wiley.com/doi/10.1111/ffe.13902 by Politecnico Di Torino Sist. Bibl Del Polit Di Torino, Wiley Online Library on [09/02/2023]. See the Terms and Conditions (https://onlinelibrary.wiley.com/terms-and-conditions) on Wiley Online Library for rules of use; OA articles are governed by the applicable Creative Commons License

specimens under four point bending. *Int J Solids Struct*. 2018; 143:175-182.

43. Chouchaoui BA, Pick RJ. Behaviour of longitudinally aligned corrosion pits. *Int J Press Vessel pip*. 1996;67(1):17-35.
44. Hou J, Song L. Numerical investigation on stress concentration of tension steel bars with one or two corrosion pits. *Adv Mater Sci Eng*. 2015;2015:1-7.

How to cite this article: Ferrian F, Chao Correas A, Cornetti P, Sapora A. Size effects on spheroidal voids by Finite Fracture Mechanics and application to corrosion pits. *Fatigue Fract Eng Mater Struct*. 2023;46(3):875-885. doi:10.1111/ffe.13902

14602695, 2023, 3, Downloaded from https://onlinelibrary.wiley.com/doi/10.1111/ffe.13902 by Politecnico Di Torino Sist. Bibl Del Polit Di Torino, Wiley Online Library on [09/02/2023]. See the Terms and Conditions (https://onlinelibrary.wiley.com/terms-and-conditions) on Wiley Online Library for rules of use; OA articles are governed by the applicable Creative Commons License